Coverage-Dependent Modulation of Charge Density at the Interface between Ag(001) and Ruthenium Phthalocyanine

Giuseppe Mattioli, Giorgio Contini, Fabio Ronci, Roberto Flammini, Federico Frezza, Rosanna Larciprete, Venanzio Raglione, Paola Alippi, Francesco Filippone, Aldo Amore Bonapasta, et al.

Coverage-Dependent Modulation of Charge Density at the Interface between Ag(001) and Ruthenium Phthalocyanine

Giuseppe Mattioli,* Giorgio Contini, Fabio Ronci, Roberto Flammini, Federico Frezza, Rosanna Larciprete, Venanzio Raglione, Paola Alippi, Francesco Filippone, Aldo Amore Bonapasta, Gloria Zanotti, Bertrand Kierren, Luc Moreau, Thomas Pierron, Yannick Fagot-Revurat, and Stefano Colonna*

ABSTRACT: When an organic film is deposited on a metal surface, charge layers are formed at the interface. These are an important feature of the interface electronic structure and play a crucial role as separation layers between electrodes and active layers in organic devices. Here, we report on a study of the interface between diruthenium phthalocyanine, $(RuPc)_2$, and the Ag(001) surface. The molecules form two different commensurable arrangements on the substrate, a low density one for a coverage well below the first monolayer and a high density one up to the completion of the monolayer. The focus of this study is on the interface states evolution with the molecular density on the metal surface and the charge distribution in the thin interfacial layer between molecules and substrate. From this investigation, conducted by low energy electron diffraction, scanning tunneling microscopy/spectroscopy, photoemission spectroscopy, and density functional theory, we have found that, even if individual molecules are characterized by a quite similar surface-to-molecule charge transfer pattern, the two molecular arrangements present different valence band structures and, more interestingly, different modulations of the interface charge. These charge modulations are governed by interfacial states energetically resonant with the molecular states, localized at the position of the molecules as well as by a reaction of the electronic cloud of the metal surface to the molecular adsorption due to a Pauli pushback effect. This complex, spatial charge modulation makes the $(RuPc)_2$/Ag(001) an interesting case of interaction intermediate between physisorption and chemisorption.

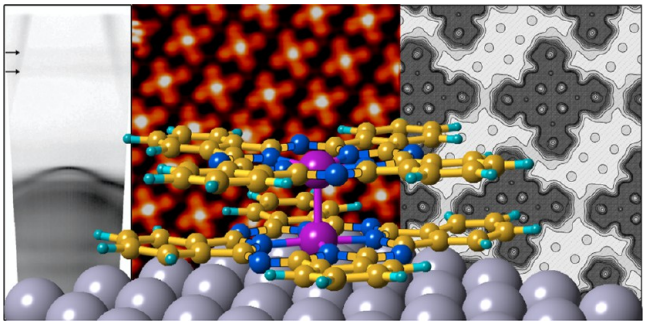

INTRODUCTION

The rich variety of physical and chemical phenomena involved in the formation of hybrid organic−inorganic interfaces has been the subject of intense research. In particular, organic−metal interfaces take center stage because of their crucial role as separation layers between electrodes and active materials in organic devices.[1] In this flourishing research field, low index surfaces of coinage metals are frequently used in combination with archetypal organic molecules like pentacene, naphthalene tetracarboxylic anhydride, perylene tetracarboxylic dianhydride, and metal phthalocyanines.[2−11] In particular, this last class of molecules is largely explored in hybrid interfaces, because of the thermal stability and the possibility to tailor the properties by changing the central metal atoms or functionalizing the organic macrocycle.

When an organic film is deposited on a metal surface, charge layers are formed at the interface,[12,13] determining its electronic behavior. The charge distribution at such an interface and its energetics depend on the degree of interaction between the molecule and the metal substrate. In a low interaction regime (physisorption), an exchange-like interaction between the metal and molecular electron clouds modulates the interface charge density.[14,15] Increasing the interaction to the limit of chemisorption, hybridization between metal and molecular electronic states takes place, resulting in broadening and/or splitting of the involved molecular orbitals.[16−18]

Interestingly, in some organic-metal interfaces the molecular arrangement may change as a function of the molecular amount. During the growth of the first monolayer (ML) of organic molecules on different substrates, rich phase diagrams have been found exhibiting disorder−order transitions, differ-

Received: November 28, 2022
Revised: January 24, 2023

ent disordered or ordered arrangements that can be commensurable or not with the substrate lattice, and, in some cases, more complex point-on-line arrangements.[19] The different molecular lattices formed at the interfaces can be accompanied by changes of the molecule−substrate interaction as testified by the change in the molecular distance from the surface or the interaction strength.[2,4,8] On the other hand, the consequent evolution of the interface electronic structure with the molecular deposition is by far less investigated, in particular in the case of different arrangements of the molecules as a function of the molecular density, yet the electrostatic interactions between the molecules can produce a rich set of phenomena that influence the molecular orbitals and the interface states.[20−27]

In this paper, we report on the study of the interface between diruthenium phthalocyanine ($(RuPc)_2$ hereafter) and the Ag(001) surface. The focus of this investigation is on the interface states, that is, the electronic states localized between the metal surface and the organic layer, and their evolution with the molecular density on the metal surface. The interest for $(RuPc)_2$ in this context has been stimulated by its peculiar magnetic properties and the additional degree of freedom induced by its rotamerism.[28] Indeed, $(RuPc)_2$ is a double decker phthalocyanine molecule composed of two RuPc monomers connected by a direct Ru−Ru bond. The free molecule presents two stable rotamers characterized by two different rotation angles between the two monomers.[28] This almost unique structure of a double decker phthalocyanine presents an electronic structure characterized by two unpaired electrons coupled in a triplet state conferring interesting paramagnetic properties to the molecule. The Ag(001) substrate, on the other hand, has been chosen because the square symmetry of its surface is expected to favor the self-assembling of the phthalocyanine quadrilobate units, which naturally tend to form square molecular arrangements.[29−32] Moreover, the Ag(001) does not present surface states close to the Fermi level that can interfere with the formation of interface electronic states, as frequently observed for the (111) surfaces of metal substrates, thus simplifying the study.[33] Due to the ability of $(RuPc)_2$ to form ordered assemblies on noble metal surfaces already at the sub-ML stage,[34] $(RuPc)_2$/Ag(001) appears as the ideal playground for the investigation of the connection between electronic structure and surface molecular arrangement. From this study, conducted by low energy electron diffraction (LEED), scanning tunneling microscopy/spectroscopy (STM/STS), core level (XPS) and angle resolved photoemission spectroscopy (ARPES), and density functional theory (DFT), we have found that the molecules form two different commensurable arrangements on the substrate, a low density one for a coverage well below the first monolayer and a high density one up to the completion of the first monolayer. A different valence band structure is observed for the two molecular arrangements. Moreover, the charge density modulation along the interfacial plane changes with the molecular structure, being governed by interfacial states resonant with the molecular states, localized at the position of the molecules, as well as a complex spatial charge modulation due to a Pauli pushback effect. These evidences demonstrate that the $(RuPc)_2$/Ag(001) is an interesting case where the metal−organic interaction intermediate between physisorption and chemisorption leads to a multifaceted interface charge arrangement.

METHODS

The $(RuPc)_2$ synthesis was conducted as reported in ref 35 (see also the Supporting Information for a more detailed description of the synthetic procedure) and twice purified by vacuum sublimation. The experiments were conducted by using two different ultrahigh vacuum chambers, one for STM and one for photoemission spectroscopy measurements. Both chambers were equipped with a LEED optics (LEED/Auger in the case of STM chamber). The Ag(001) single crystal was prepared by several cycles of Ar^+ ion sputtering and annealing. The surface quality was verified by LEED, Auger or photoemission spectroscopy and STM. The $(RuPc)_2$ layers were prepared in the photoemission and microscopy chambers by following the same well-established procedure. Molecules were sublimated at a temperature of about 400 °C on the silver substrate held at room temperature (RT). The deposition cells were thoroughly outgassed before the experiments in order to ensure a background pressure during the sample preparation in the low 10^{-10} mbar range. The time necessary to form a molecular monolayer (ML) on the substrate was determined following two different procedures. In the STM apparatus, the time to complete a ML was measured by an iterative procedure increasing the deposition time and inspecting the organic layer morphology by STM until the ML formation. In the photoemission apparatus, the molecular flux was measured by a quartz crystal microbalance.

LEED patterns of the molecular films were acquired at room temperature. STM measurements were performed at 80 K using electrochemically etched tungsten tips cleaned in the vacuum chamber by electron bombardment. The STM scanner was calibrated by using the bare Ag(001) atomic lattice as reference. STS and differential conductance images were acquired by adding a modulation of few mV at a frequency around 1 kHz on the bias voltage and collecting the signal by a lock-in amplifier.

The ARPES and XPS experiments were performed at RT and 5 K by using a VG-SCIENTA DA30-L analyzer. The photoemission device is equipped with a monochromatized X-ray source and a helium lamp. The energy resolution is about 300 meV for XPS and better than 10 meV for ARPES. All ARPES measurements were performed with unpolarized light.

DFT simulations have been performed by using the Quantum-ESPRESSO suite of programs[36,37] in a plane wave/pseudopotential framework. We applied a well-established yet accurate setup,[28,34] suitable for the treatment of large organic−inorganic systems containing, in this case, up to 4232 electrons in an open-shell electronic configuration. In detail, geometry optimization runs have been performed by using the C09[38] gradient corrected functional coupled with an ab initio VDW-DF[39,40] correction (C09+VDWDF). The C09+VDWDF method provides reliable description of structures and interaction energies of noncovalent organic−inorganic interfaces.[18,28,29,34,41] The Kohn−Sham orbitals have been expanded on a plane-wave basis set, with core electrons replaced by ultrasoft pseudopotentials.[42] Satisfactorily converged results have been obtained by using cutoffs of 40 Ry (320 Ry) on the plane waves (electronic densities). The range-separated HSE[43,44] hybrid functional is particularly suitable for the calculation of electronic properties of metal−organic interfaces.[45−48] Its formulation introduces in the DFT exchange-correlation part an exact-exchange (EXX) nonlocal contribution, which corrects delocalization errors[49,50] without opening

spurious gaps in metallic systems, thanks to the vanishing EXX contribution at long-range, with an overall performance not unlike that obtained by using many-body perturbation theory methods such as G_0W_0.[46] Single point simulations have been therefore performed at the HSE level of theory on C09+VDWDF optimized structures. Optimized norm-conserving Vanderbilt pseudopotentials[51,52] have been used in this case to replace core electrons, together with 80/320 Ry cutoffs.

Six-layer slabs have been cut out from the bulk crystal structure to simulate the Ag(001) metal substrate. They have been separated by a significant amount of vacuum space (up to 46 Å) from their periodically repeated image along the z axis. However, the strong vertical dipole, due to interfacial charge transfer between Ag and $(RuPc)_2$ and interacting with its periodically replicated image along the z axis, can heavily affect the reliability of the simulations. We have therefore applied open boundary conditions along the z axis, embedding the active simulation space between two semi-infinite effective screening media (ESM).[53−55] Different square and monoclinic supercells, fully periodic in the (x,y) plane, have been used to simulate the different regimes of molecular coverage identified by LEED and STM measurements. They are all shown in Figure S7 in Supporting Information. The slabs have been fully optimized by using the Γ point for the sampling of the Brillouin zone and then the lowest three-layers have been kept fixed in further calculations. Only four atomic layers have been used to represent Ag substrates in the case of single-point HSE calculations.

RESULTS AND DISCUSSION

In Figure 1, a sequence of LEED patterns and constant current STM images is reported, showing the evolution of the $(RuPc)_2$ layer on the Ag(001) substrate as a function of the deposited amount. A LEED pattern is detected, though with diffused spots and a sizable background, already at the lowest deposition of 0.3 ML (Figure 1a). Increasing the molecular amount to 0.6 ML (Figure 1b), a different pattern is observed which, however, appears quite blurred and with an intense background, the fingerprint of a sample surface composed of small organized domains. At 1 ML the same LEED pattern as in 0.6 ML sample is obtained but much sharper and with a low background (Figure 1c), demonstrating that the complete organic layer is composed of large and well ordered domains. We will refer to as low-density and high-density structures, hereafter, for the molecular arrangements below and above 0.6 ML, respectively. Further, increasing the deposition to a multilayer film a blurred LEED pattern is obtained (Figure 1d), evidence of a quite disordered arrangement of $(RuPc)_2$. The STM image of the 0.3 ML sample (Figure 1e) presents some stripes and the uncovered areas appear hazy. This happens because, even at 80 K, the molecule mobility is high, preventing the acquisition of high resolution images of the molecular islands. This observation is in agreement with the intense background and diffused spots in the LEED pattern of the same sample (Figure 1(a)). In the 0.6 ML sample (Figure 1f), a molecular layer formed by several ordered domains, tens of nanometers wide, is obtained. At 1 ML (Figure 1g) the molecular layer is virtually complete, and the surface is well ordered with the molecules arranged in large monoclinic domains with different orientations dictated by the 4-fold symmetry of the Ag(001) substrate. It is possible to observe small patches of the bare substrate (the darkest regions) and few molecules located at the second layer (the bright features). The STM images of the 0.6 and 1 ML show that the molecular arrangement in the ordered domains is the same for the two coverages, in agreement with the LEED patterns in Figure 1, parts b and c. When increasing the deposition to 1.5 ML (Figure 1h), the first monolayer of molecules is completed and ordered molecular islands, a few tens of nanometers wide, start assembling at the second layer, whose structure is different from that of the first layer (see the insets h′ and h″). Whereas the structure of the first layer will be discussed below, here it is worth noting that the molecules in the second layer tend to form a square lattice, an arrangement that has been demonstrated to be the most favorable when the interaction between the $(RuPc)_2$ molecule and the substrate is low.[28] Accordingly, we can explain the observed square arrangement of the second layer domains by a weaker interaction between the molecules of the first and second layer than between the first layer molecules and the metal substrate. At very high coverage (more than 4 ML), several molecular layers are present on the surface, and the STM images show mostly a disordered structure with a few ordered islands having square symmetry (Figure 1i), in agreement with the blurred LEED pattern in Figure 1d.

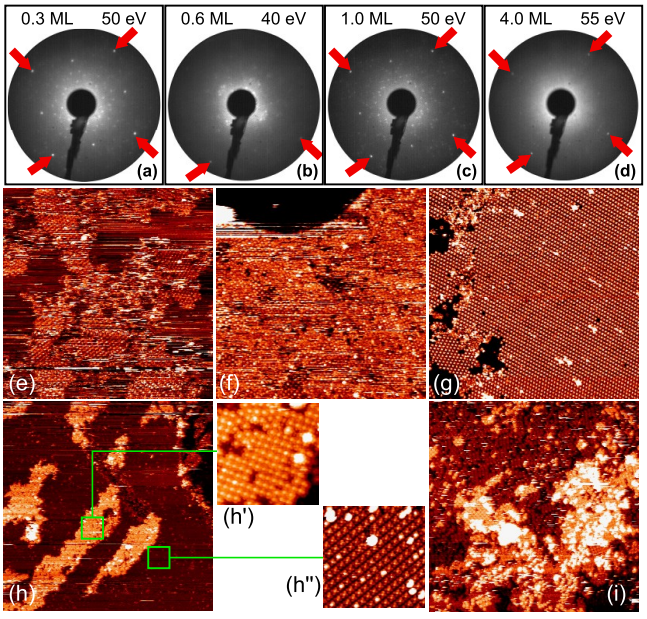

Figure 1. LEED patterns (a−d) and constant current STM images (e−i), showing the evolution of the surface structure when increasing the $(RuPc)_2$ deposition on Ag(001). The red arrows in the LEED patterns indicate the Ag(001) spots. (e) 0.3 ML, 100 × 100 nm^2, −2.2 V, 1.5 nA. (f) 0.6 ML, 100 × 100 nm^2, +0.2 V, 2 nA. (g) 1 ML, 100 × 100 nm^2, −2.5 V, 3 nA. (h) 1.5 ML, 250 × 250 nm^2, + 2 V, 2 nA. The insets show 20 × 20 nm^2 images of the molecular structure of the first and second layer. (i) More than 4 ML, 100 × 100 nm^2, +2 V, 0.05 nA.

In Figure 2 the LEED patterns of the 0.3 and 1 ML samples are reported from which we worked out the $\begin{pmatrix} 2 & -6 \\ 6 & 2 \end{pmatrix}$ and $\begin{pmatrix} 5 & 3 \\ -1 & 5 \end{pmatrix}$ overlayer matrices for the low- and high density structure, respectively. In the corresponding reciprocal lattices,[56] reported in Figure 2 superimposed on the LEED patterns, the different colors of the markers indicate the different symmetry-equivalent domains on the surface. In the same figure a sketch of the two molecular structures is

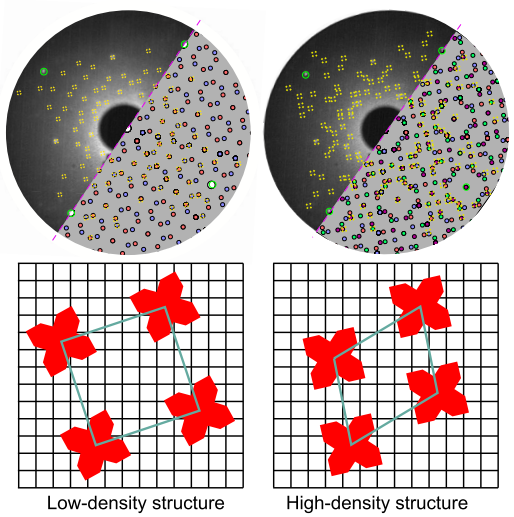

Figure 2. Top, LEED patterns collected on the 0.3 ML (left) and 1 ML (right) samples, compared to the calculated reciprocal lattice of the molecular overlayers (lower right half of the images). The green circles indicate the position of the bulk spots and the yellow markers highlight the position of the LEED spots. The different colors of the reciprocal space points indicate the different symmetry related domains. Bottom, sketch of the two molecular arrangements.

reported. More details about the structural analysis are reported in the Supporting Information (see Figures S1 and S2).

The surface molecular densities calculated for the low- and high-density structures are $\rho_{ld} = 3.0 \times 10^{13}$ cm^{-2} and $\rho_{hd} = 4.5 \times 10^{13}$ cm^{-2}, respectively. These values indicate that at 0.3 ML the molecules form organized self-assembled islands surrounded by large regions of bare substrate. Indeed, if the molecules were uniformly distributed on the substrate, we would expect a surface density of about one-third with respect to the 1 ML sample. On the contrary, the ratio between the experimental densities, $\rho_{ld}/\rho_{hd} = 0.66$, is significantly higher. This observation indicates that intermolecular interactions lead to molecular self-assembling starting from the first stages of the interface formation.

From the combined LEED and STM measurements, it is possible to outline the development of the interface and the mechanisms involved in its formation. At very low coverage, the molecules self-assemble in sparse, ordered low-density structures. In this regime, even though the molecular density is very low, intermolecular interactions are strong enough to influence the molecular organization, leading to the formation of islands of molecules having surface density much higher than the nominal coverage, coexisting with regions of bare metal surface. The enlargement of the domains upon further molecular deposition is favored by the mobility of the molecules on the substrate that are easily included in the formed domains. Because the molecules on the second layer have a weaker interaction with the first layer ones, they can diffuse above the formed domain. When they arrive at boundaries, they drop down and can be also incorporated in the first layer domain. As the molecular coverage increases toward the complete ML, the ordered domains are forced to switch toward the high-density structure to accommodate a larger amount of molecules in direct contact with the surface. This can explain why at intermediate coverage we observe small domains of high-density structure (see Figure 1f). Then, as the growth proceeds, larger domains grow at the expense of smaller ones, eventually forming a complete layer (see Figure 1, parts c and g). Such qualitative considerations based on LEED and STM data will be quantified on the grounds of theoretical results discussed below. However, we understand that $(RuPc)_2$/Ag(001) represents an interesting organic/metal interface whose structure changes as a function of the molecular coverage. In order to ascertain to which extent the charge rearrangements at $(RuPc)_2$/metal interfaces[34] are influenced by the molecular distribution on the surface, we have comprehensively investigated the interface electronic structure. To this aim, we have carried out systematic core and valence photoemission spectroscopy measurements at the different stages of the interface formation. XPS measurements show, as expected, an intensity decrease of the Ag 3d peaks as the deposition time is increased, with a concomitant increase of the C 1s peak intensity, which is partially overlapped with the Ru 3d spectral region (see Figures S3 and S4). The C 1s peak presents different contributions and, similarly to previous phthalocyanine investigations,[57−59] has been deconvoluted by five components plus components related to Ru $3d_{3/2}$ (see Figure S5). Thanks to the significant spin−orbit splitting of the Ru 3d peak ($\Delta \approx 4.2$ eV) the Ru $3d_{5/2}$ component is well resolved from the C 1s manyfold allowing a reliable analysis. The evolution of the Ru $3d_{5/2}$ peak line-shape as a function of the molecular layer thickness is reported in Figure 3. Each spectrum has been deconvoluted using a Shirley background plus one to three components coming from Ru atoms in different oxidation states. At low coverage ($\leq$1 ML) a single component is observed (first component; green line).

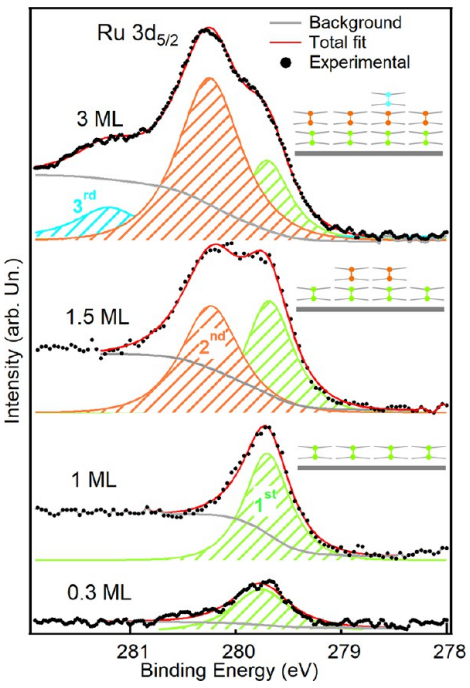

Figure 3. XPS measurements at the Ru $3d_{5/2}$ peak as a function of the molecular deposition. The dots are the experimental curves, the hatched regions represent the different components of the fit, the gray line the Shirley function used to simulate the background and the red line is the resulting fit. In the insets the molecules contributing to the different components are schematically illustrated. The spectra are normalized to the intensity of the Ag 3d peak.

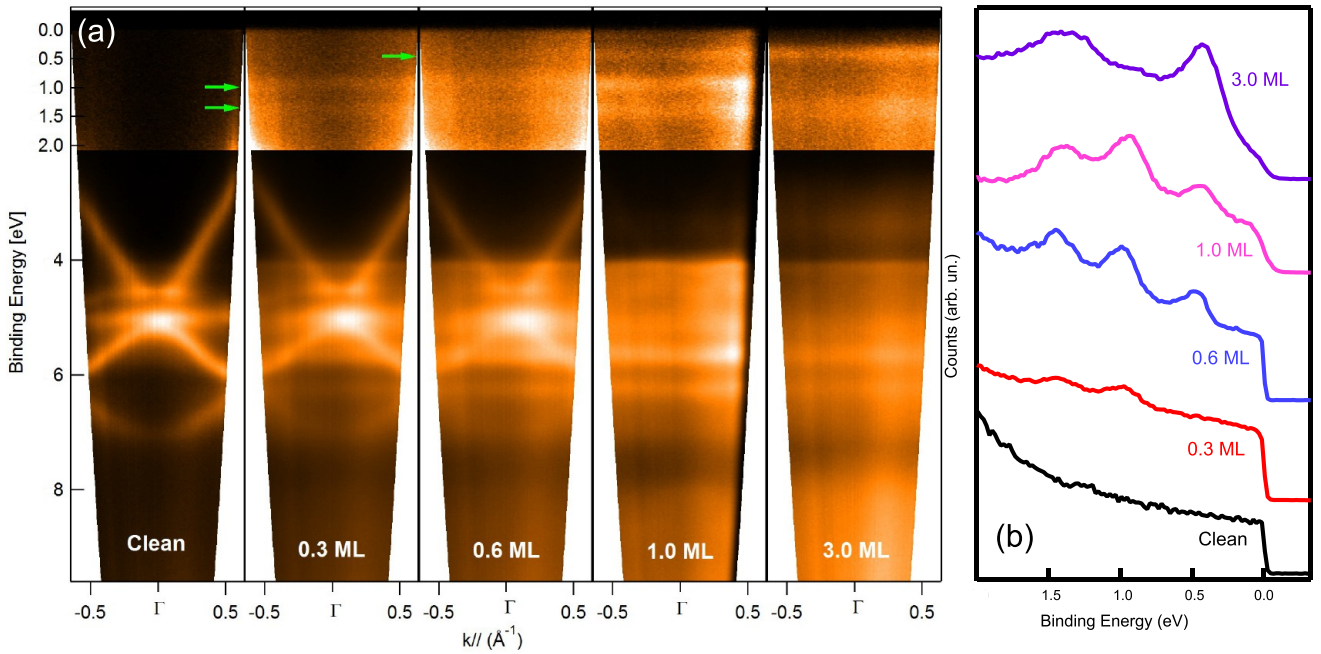

Figure 4. (a) ARPES maps of $(RuPc)_2$/Ag(001) at increasing molecular coverage, collected along the $\bar{\Gamma}-\bar{X}$ direction of the Ag(001) substrate. The contrast in the binding energy range between E_F and 2.0 eV has been enhanced by a factor of 5 in order to better display the molecular states. (b) Valence band spectra integrated around the $\bar{\Gamma}$ point for different molecular depositions.

Additional components at higher binding energies are observed in going toward multilayer coverage.

The component at lower binding energy (≈279.7 eV) is assumed to be related to ruthenium in an oxidation state close to Ru^0.[60] This reduced state of the Ru atoms is ascribed to the contact of the molecules with the silver surface, which induces a surface to molecule charge transfer mainly involving the Ru atoms, also observed in the case of other metal substrates.[34,61] Increasing the molecular deposition to about 1 ML, we observe an increase of the Ru signal but no new components in the spectrum. At a coverage of about 1.5 ML, the spectrum shows a second component (orange line) around 280.2 eV. Further increasing the molecular coverage to 3 ML, the second component becomes predominant and a third one is observed at an even higher binding energy of 281.2 eV (blue line). The last two components are both compatible with ruthenium in a 2+ oxidation state,[62] as expected in the neutral $(RuPc)_2$ molecule. The evolution of the Ru XPS peak can be interpreted in light of the STM images in Figure 1. The Ru $3d_{5/2}$ component at low binding energy can be attributed to the molecules directly in contact with the substrate. The energy position of the single component in spectra for the 0.3 and 1 ML is the same within the energy resolution of our experimental setup. This observation indicates that the metal to molecule charge transfer is the same for the low- and high-density structures. The second component at higher binding energy, observed when the molecular layer thickness is increased, can be attributed to the molecules located on the second layer (see Figure 1, parts h and h′), partially interacting with the substrate. Lastly, the component at the highest binding energy, observed on the 3 ML sample, can be assigned to the molecules located in the third layer, electronically decoupled from the substrate. The peak is in fact closely compatible with that measured in the case of $(RuPc)_2$ deposited on graphite (≈ 281.2 eV), where the interaction between molecules and substrate is negligible.[28,34]

In Figure 4a, ARPES maps collected around the $\bar{\Gamma}$ point (along the $\bar{\Gamma}-\bar{X}$ direction) of the Ag(001) surface Brillouin zone are reported, measured on samples with different molecular amounts. In the Supporting Information (Figure S6), ARPES maps collected around the $\bar{M}$ point (along the $\bar{\Gamma}-\bar{M}$ direction) are also reported for completeness (see also Figure S6 for a scheme of the Ag(001) Brillouin zone). Here the maps around $\bar{\Gamma}$ are discussed for a direct comparison with the STS spectra and theoretical calculations reported below. The clean silver surface shows dispersing d bands in the region below 4 eV, while sp bands are observed closer to the Fermi level. After the $(RuPc)_2$ deposition, some flat bands arising from the molecular overlayer emerge, clearly visible in the binding energy region from the Fermi level down to about 6.5 eV. Increasing the molecular amount on the silver surface, the intensity of the molecular features increases and when the coverage reaches 3 ML the silver electronic structure is completely obscured by the molecular layer. It is interesting to note that, close to the Fermi level, for the lowest molecular deposition, two features (around 1 eV and 1.4 eV, respectively; highlighted by green arrows) are observed. When the molecular deposition is increased to 0.6 ML and the molecular layer switches to the high-density structure, the presence of a third peak is observed around 0.5 eV. This evolution of the interface electronic structure around the Fermi level is even better illustrated in Figure 4b, where the valence band photoemission spectra integrated around the $\bar{\Gamma}$ point are reported. This evolution of the valence band closely follows the structural phase transition suffered by the molecular layer observed by LEED (Figure 1), where two different patterns are observed below and around the monolayer. When the molecular amount is increased above one monolayer the energy position of the peaks remain the same but the

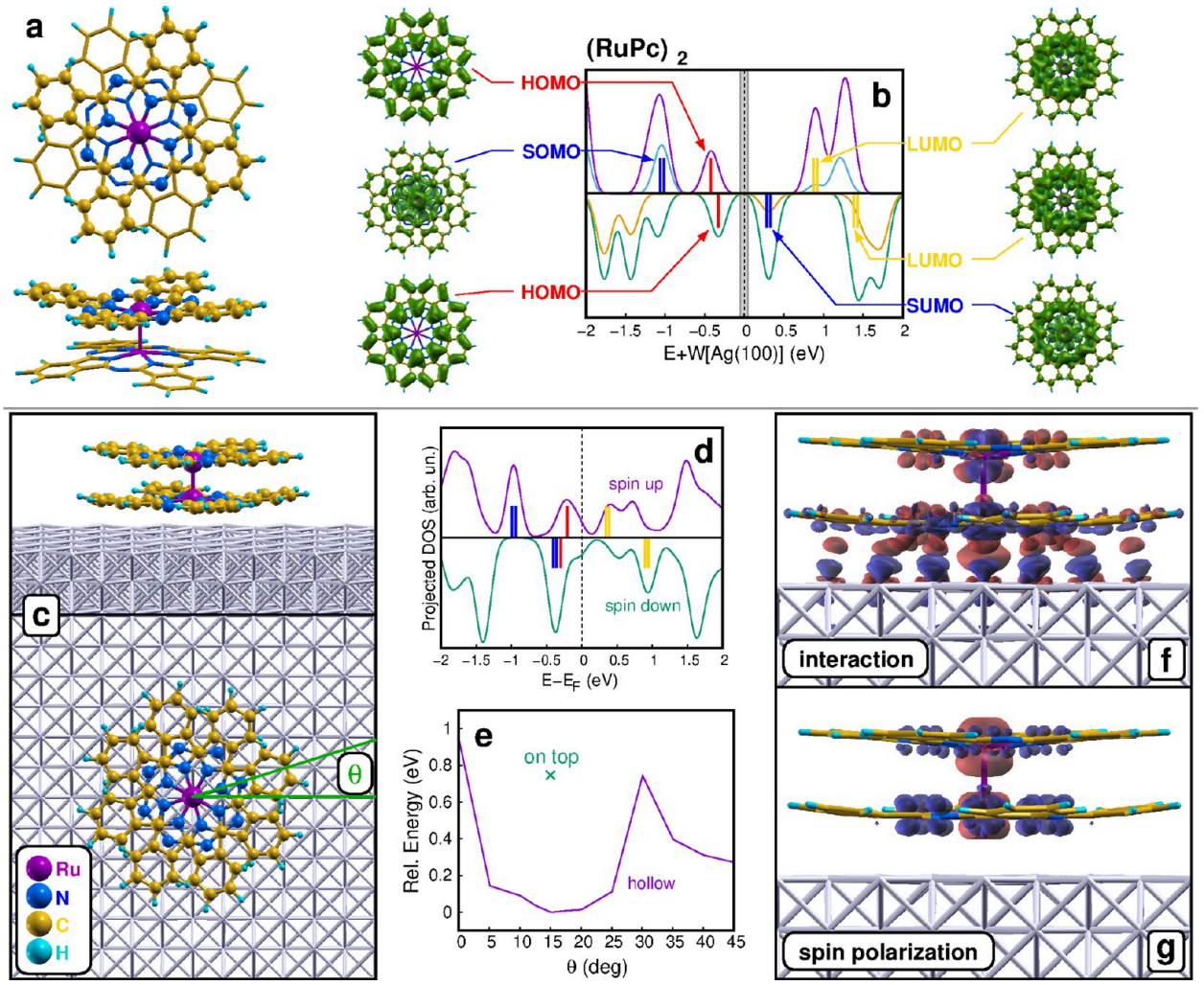

Figure 5. (a) Equilibrium geometry of the staggered $(RuPc)_2$ (top and side view). To facilitate the visualization of the molecular structure the two monomers are shown as skeleton and ball-and-stick models, respectively. (b) Spin resolved total and projected on Ru 4d orbitals density of states of a $(RuPc)_2$ molecule in gas phase. Occupied and unoccupied orbitals are separated by a thin dashed line. A silvery band indicates the typical region of the measured Ag(001) Fermi level, taken as reference value of the energy scale. Frontier orbitals are indicated as colored bars. The corresponding $|\psi|^2$ plots are also shown. (c) Equilibrium geometry (top and side view) of an isolated $(RuPc)_2$ interacting with the Ag(001) surface. (d) Spin-resolved density of states of the same system, projected on $(RuPc)_2$ orbitals (bars defined in panel b). (e) Relative adsorption energy of $(RuPc)_2$ on Ag(001) hollow site as a function of the angle θ between the Ru–N bond and the [010] direction of the surface (see also panel c for the definition of θ). A single light green cross marks the adsorption energy of the most stable configuration of the on top adsorption. (f) Map of the charge density displacement blue (red) indicating charge depleted (accumulated) regions. (g) Spin polarization map of the interacting system, Red (blue) indicate accumulation of spin up (down). For both panels f and g, the sampling is 0.002 au^{-3}.

structures around 0.6 and 1.4 eV gain intensity with respect to the third one.

In order to interpret and rationalize the experimental results, a thorough theoretical modeling of the $(RuPc)_2$/Ag(001) interface at different coverages has been undertaken. Such a computational investigation may conveniently start from a short description of the electronic properties of a $(RuPc)_2$ molecule in gas phase, taken as reference. The peculiar structure of $(RuPc)_2$ in which two RuPc monomers are kept together by a stable Ru–Ru bond, almost unique in the large class of phthalocyanine molecules, is shown in Figure 5a. The free molecule has two stable structures, staggered and semieclipsed, with the two monomers rotated by 45° and 15°, respectively. In the free molecule, these two rotamers present almost the same energy and are separated by a low energy barrier.[28] However, we anticipate that when the molecule is in contact with the silver surface, the semieclipsed rotamer becomes 0.6 eV less stable than the staggered one.[34] Therefore, only results related to the latter will be discussed below. The $(RuPc)_2$ frontier orbitals can be divided in two different contributions, described in detail in Figure 5b. Conventional HOMO (red bars) and LUMO (yellow bars) orbitals, mainly involving the π-conjugated Pc ligands, are 2-fold degenerate according with the D_{4d} symmetry of the molecule and relatively insensitive to spin differences. Two more peculiar sets of orbitals, the singly occupied molecular orbital (SOMO) and singly unoccupied molecular orbital (SUMO) (blue bars), are characterized by a larger contribution of Ru 4d atomic orbitals (spin-up and spin down contributions shown as light blue and orange curves, respectively) and are mainly responsible for the magnetic properties of the isolated $(RuPc)_2$.

Periodic boundary conditions have been exploited to simulate different molecular coverages on the Ag(001) surface.

Table 1. Valence Atomic Charge (Total) and Spin Polarization (pol), Expressed in au, of the Upper and Lower Ru atom, the Upper and Lower Pc Ligands, and the Whole $(RuPc)_2$ Molecule[a]

Bader's Charge / Polarization	Ru		Pc		$(RuPc)_2$				
	lower	upper	lower	upper	lower	upper	total	pol	abs
$(RuPc)_2$	14.93	14.93	185.07	185.07	200.00	200.00	400.00	2.00	2.00
gas-phase	0.87	0.87	0.13	0.13	1.00	1.00			
$Ag/(RuPc)_2$	15.12	14.94	185.67	185.44	200.79	200.38	401.17	0.18	1.98
isolated	0.32	0.76	-0.62	-0.28	-0.30	0.48			
$Ag/(RuPc)_2$	15.07	14.98	185.65	185.50	200.72	200.48	401.20	0.12	1.91
low-density ML	0.33	0.69	-0.60	-0.29	-0.27	0.40			
$Ag/(RuPc)_2$	15.00	14.99	185.80	185.50	200.80	200.49	401.29	0.14	1.90
high-density ML	0.36	0.66	-0.62	-0.26	-0.26	0.40			
$Ag/(RuPc)_2$	14.97	15.01	184.90	185.11	199.87	200.12	399.99	0.52	1.48
2nd-layer	0.37	0.63	-0.24	-0.24	0.13	0.39			

[a]Values calculated at the HSE@PW level of theory by using the Bader's partitioning method in the cases of a gas-phase molecule, an isolated molecule deposited on the Ag(001) substrate, an ordered layer (low- and high-density), and an isolated 2nd layer molecule. The abs value (printed in blue) is the sum of absolute values of the Ru and the ligand (C, N, and H atoms) spin polarization (printed in red).

The corresponding surface cells are shown in Figure S7. The equilibrium structure of an isolated $(RuPc)_2$ molecule in contact with the Ag(001) surface is shown in Figure 5c. The adsorption is favored when the Ru−N(pyrrole) bond of the first monomer (the one in contact with the substrate) forms an angle of about 15° with the ⟨100⟩ direction of the Ag substrate and the Ru−Ru axis is placed on a square hollow site (see the energy profile reported in Figure 5e). The interaction of the molecule with the Ag surface stabilizes the staggered rotamer and induces a strong rearrangement of its charge. In Figure 5d, the densities of electronic states projected on molecular orbitals (PDOS) are reported. The conspicuous effect of the contact of an isolated molecule with the Ag substrate is the displacement of the SUMO — spin down — below the Fermi level, which accommodates the charge transferred from the Ag substrate to the molecule. As a consequence the Ru atoms are reduced (cf. Figure 3 for the experimental support to this observation) and their spin polarization strongly decreased. On the other hand, two concomitant effects contribute to the accumulation of spin down charge on Pc ligands: the charging itself of the spin-down SUMO orbitals, which are participated in by ligand atoms, as shown in Figure 5b, and the opposite tendency of the spin up HOMO, which moves closer to the Fermi level, tailing in the empty states region. These phenomena are clearly visualized in Figure 5f, where a map of the charge density displacement is reported. The map is obtained by subtracting from the electronic density of the metal−molecule interacting system the electronic density of the two components, calculated as separate parts frozen in their interacting geometry. In other words, the electronic charge is displaced from blue to red regions as a consequence of the molecule−metal interaction. The extent of charge displacement is more pronounced on the monomer in contact with the Ag(001) surface, where we can note a charge increase in the central part of the molecule mostly involving electronic states residing on the lower Ru atom. The reduction of the metal atom is accompanied by the presence of charge depletion regions (the blue ones) mainly on the downward face of the lower macrocycle and accumulation regions in the interface space.

The charge rearrangement entails an important modification of the molecule spin polarization, as exemplified by the polarization map reported in Figure 5g, showing the difference between the spin-up and spin-down densities: red regions present an excess of spin-up density while blue ones present an excess of spin-down. It is possible to note that the spin up polarization of the lower Ru atom is reduced with respect to the upper one and that the macrocycles acquire a spin down polarization. Such changes can be quantified by the Bader partitioning analysis[63−65] reported in Table 1. The valence charge is reported for the whole molecule and separately for the two monomers (the lower one — in contact with the metal substrate — and the upper one), to better illustrate the charge and spin polarization in the $(RuPc)_2/Ag(001)$ system. The same analysis is also reported for the molecule in the gas phase for comparison. The first thing we note in Table 1 is a metal to molecule charge transfer of more than one electron that is not equally distributed between the two RuPc monomers. The lower monomer undergoes a larger charge transfer with respect to the upper one. On the other hand, within a monomer the extent of the charge transfer is different for the Ru atom and the organic ligand. Indeed, a charge increase of more that 1% of the Ru atom is accompanied by a smaller charge increase of about 0.3% of the related Pc ligand. From the data in Table 1, we also see that the lower Ru atom undergoes a sizable reduction of its spin polarization, a phenomenon also observed, to a minor extent, in the upper Ru atom. The reduction of the Ru atoms spin polarization does not point, however, to a magnetic quenching of the molecule. Indeed, we observe concomitantly an increase of the Pc spin polarization. This behavior is well understood by the absolute value of the polarization given by the sum of the absolute values of the Ru atoms and ligands, which remains very close to the value of the free molecule. Thus, the contact with the Ag substrate does not simply give rise to a reduction of the magnetism of the molecule but induces a complex magnetic polarization due to

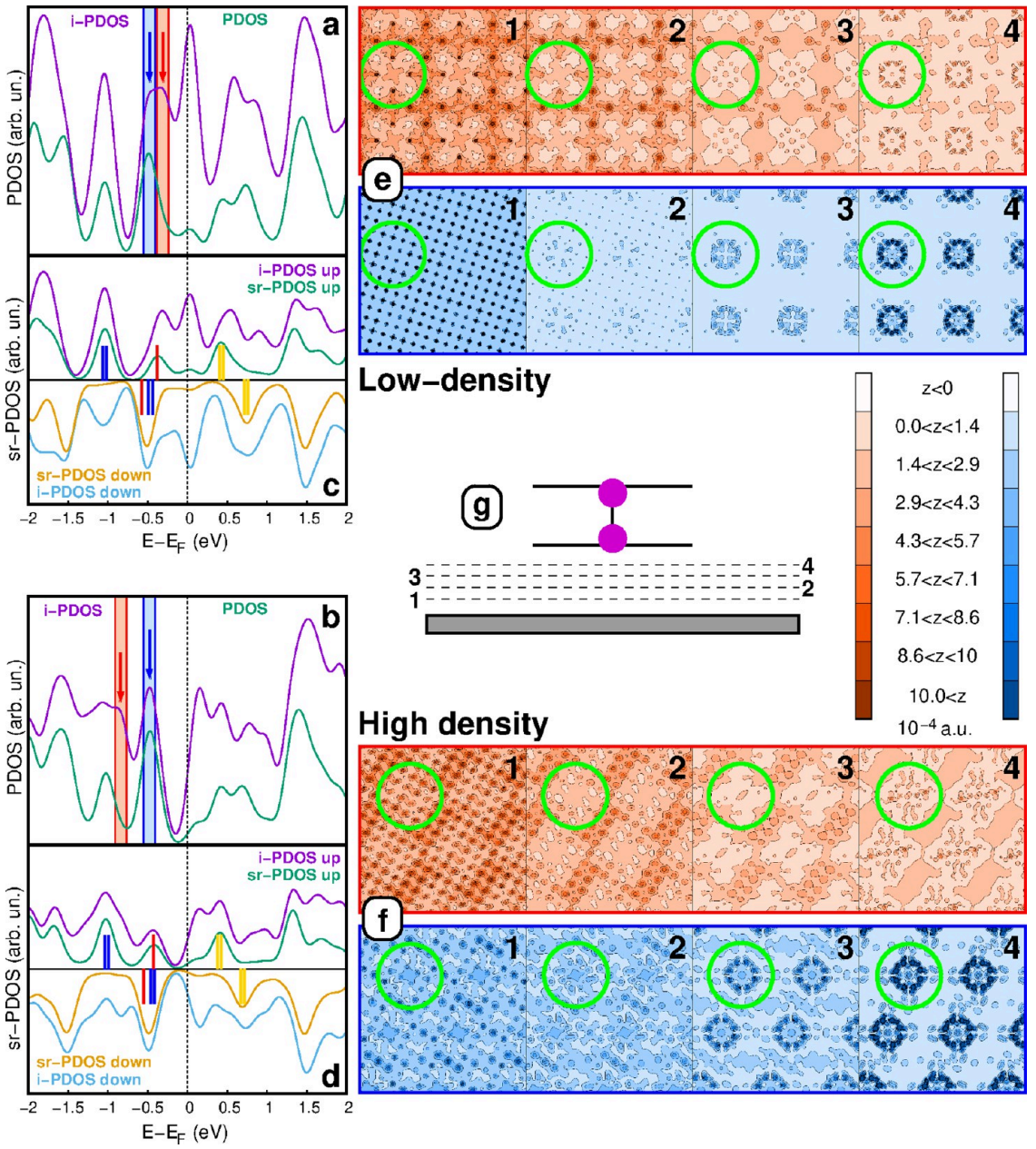

Figure 6. Total (a, b) and spin-resolved (c, d) density of states projected on $(RuPc)_2$ only (PDOS) and on $(RuPc)_2$ and Ag first layer orbitals (i-PDOS): (a, c) low-density structure; (b, d) high-density structure. The bars indicate the position of the molecular orbitals (red HOMO, blue SOMO and SUMO, yellow LUMO). Red and blue arrows in panels a and b indicate two energy regions spanning 0.2 eV of width where the i-PDOS has been integrated. Following the same color code, the maps in panels e and f report the spatial distributions of the integrated i-PDOS within planes parallel to the interface and located at different heights between the substrate and the first $(RuPc)_2$ monomer, as sketched in the inset (g). A green circle indicates the position of $(RuPc)_2$.

two different spin systems, namely the Ru atoms and the organic macrocycles.

High- and low-density equilibrium structures used for DFT calculations are reported in Figure S8. The high-density structure has been worked out by regularly placing the molecules on the Ag(001) hollow sites according to the monoclinic lattice established by the LEED measurements, and the upper monomer oriented with respect to the substrate as observed in STM images (Figure S1). Then, the lower monomer has been rotated and the molecule relaxed to find the most stable configuration. The low-density structure has been found by rotating and optimizing the whole molecule kept in its preferred staggered structure, because the orientation could not be extracted by STM images. This procedure is justified by the fact that the intermolecular spacing is larger than in the high-density lattice; thus, the intermolecular interactions do not induce rotational strain between the monomers. Slight changes in the calculated adsorption energies, corresponding to the different assemblies, can explain the alternation of different molecular lattices at increasing coverages. The adsorption energy of an isolated molecule, with negligible intermolecular interaction, has a value of 6.73 eV, in line with the value calculated using the same theoretical setup for the Ag(111) and Au(111) surfaces.[34] In the case of the low-density square lattice, the adsorption energy is increased to 6.97 eV per molecule. Such

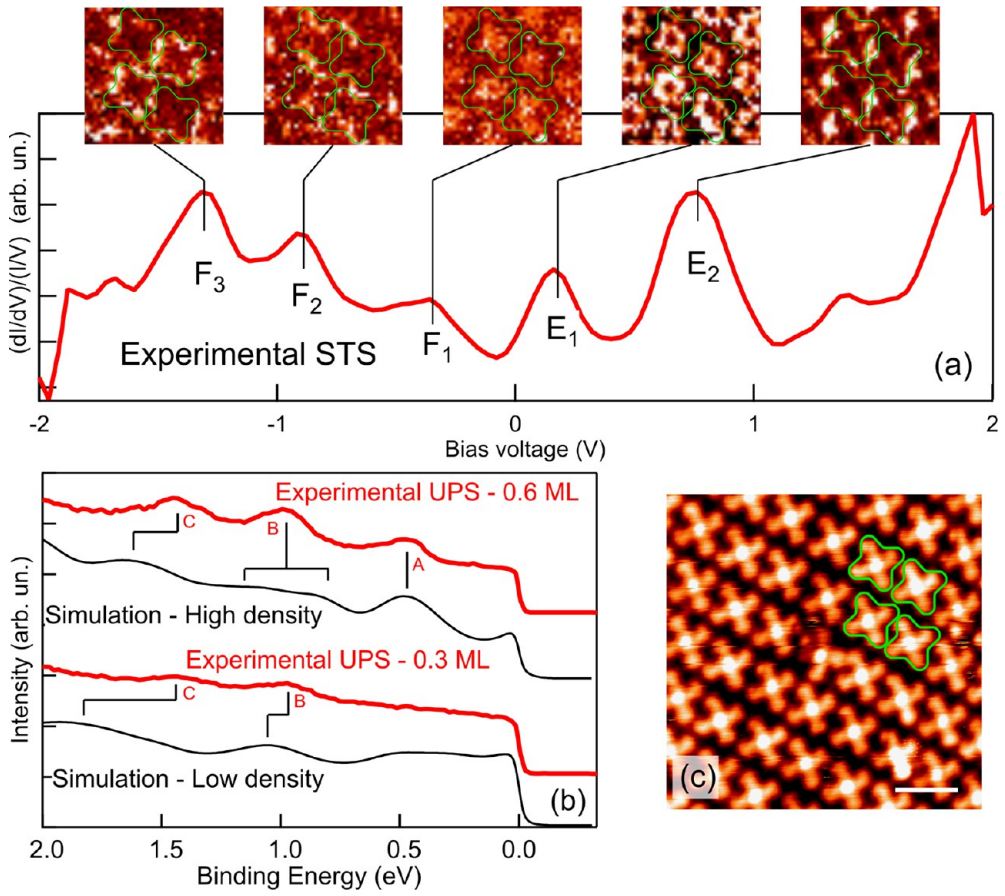

Figure 7. (a) Normalized STS spectrum obtained by averaging different spectra collected on a $(RuPc)_2$ monolayer. The insets report differential conductance images collected at the bias voltages of the marked peaks, the green contours indicate the position of the molecules in the layer as measured in the constant current topography image in panel c. (b) Valence band photoemission spectra for the 0.3 and 0.6 ML samples (red lines) compared to simulated spectra (black lines). (c) Constant current STM image of the $(RuPc)_2$ monolayer where the STS spectra and the differential conductance images were measured, the green contours are the reference for the insets in panel a, scale bar 2 nm.

value is compatible with the formation of square domains, induced by the free diffusion of molecules hopping among the substrate hollow sites. Sparse molecules at the second layer have a significantly lower but not negligible adsorption energy of 3.74 eV. They are, therefore, free to move on top of the first layer until they find a step leading to a more stable position, in contact with the Ag surface. At a coverage approaching the full monolayer, a phase transition from low-density square to high-density monoclinic domains is observed. A slight molecular distortion is induced in the tight-packed film, responsible for the slight lowering of adsorption energy to 6.82 eV per molecule, yet higher than the isolated value. A reduction of 3.2% in the adsorption energy is more than compensated by an increment of 50% of the molecules in direct contact with the surface, thus providing a sufficient thermodynamical driving-force for the lattice transition.

Remarkably, the values of atomic charges in all of the configurations of $(RuPc)_2$ in contact with the Ag surface are quite close (see Table 1), in agreement with XPS measurements shown in Figure 3. A further increase of the molecular deposition gives rise to the formation of subsequent molecular layers experimentally observed by STM and XPS measurements. As also reported in Table 1, the total charge of a molecule in the second layer recovers a value virtually equal to the free one. However, the molecule is not completely decoupled from the influence of the metal substrate, which induces a different spin polarization and charge distribution with respect to the molecule in the gas phase (see Table 1). This observation is in agreement with the Ru $3d_{5/2}$ XPS spectrum measured at intermediate coverage (Figure 3), showing a spectral component at binding energy between the low coverage and the multilayer, the fingerprint of molecules only partially decoupled from the substrate.

To more deeply investigate the $(RuPc)_2$/Ag(001) electronic structure, the density of states projected on the molecular states (PDOS) have been calculated. However, for a complete picture of the electronic structure it is necessary to consider the electronic states formed at the interface (see Figure 5f). Thus, the density of states projected on both molecular orbitals and atomic orbitals of Ag atoms in the first layer have also been calculated, we will refer to these curves as interface-PDOS (i-PDOS) hereafter. In Figure 6, we compare the PDOS and i-PDOS of the low- and high-density structures. Moreover, in order to evaluate the impact of the molecular packing on the molecular spin polarization, both spin integrated and spin resolved (sr-PDOS) calculations are reported. Taking into consideration the molecules packed on the surface in the square (low-density) and monoclinic (high-density) structures (Figure 6a,c and Figure 6b,d, respectively), only small changes of the PDOS are observed as also deduced from the partitioning analysis (Table 1). On the contrary, when the first Ag layer is included in the projection, switching from the

low-density to the high-density packing entails a considerable change of the i-PDOS. In particular, we note that some molecular features are strongly enhanced by a resonance with Ag states and that regions free of molecular states are populated by electronic states arising from the metal substrate. These two kinds of electronic state will be referred to as resonant and nonresonant states, respectively. At variance with the formers, the nonresonant states do not present substantial spin polarization and are differently distributed in energy in the two structures. On the grounds of these results, the comparison between the spin integrated i-PDOS and PDOS in Figure 6, parts a and b, has been performed by selecting in the plots two narrow (0.2 eV wide) energy regions including a representative, resonant electronic state (highlighted by a blue arrow) and a representative, nonresonant state (red arrow), respectively. Then, in order to investigate the properties of these two electronic states and their evolution with the molecular density, the above energy regions have been used to integrate the i-PDOS and plot their distribution along cutting planes parallel to the interface, placed at different heights between the metal surface and the first $(RuPc)_2$ monomer. In the inset (g) is schematically reported the position of these planes and the color scale of the density plots, more details about the geometry are reported in Table S1 in the Supporting Information. From the charge density distributions reported in Figure 6, parts e and f (see Figure S9 for a complete series of charge distributions cuts; in Figure S10 is also reported a sequence of total charge distribution plots for completeness), we note that when the cutting plane is placed closer to the substrate, the charge density modulation is dominated by the metal lattice. As the cutting plane gets closer to the lower monomer of the $(RuPc)_2$ molecule, the modulation of the charge density is shaped by the molecules. However, the resonant and nonresonant states present different distributions along the plane, in particular at intermediate heights between the substrate and molecule. Both for the low- and high-density structures the nonresonant state has the tendency to accumulate away from the region occupied by the molecule, being quite depleted directly below the molecule itself. This is a clear signature of the Pauli pushback effect due to the interaction between the electron rich molecular π states and the electronic states spilling out of the metal surface.[14] On the contrary, the resonant state is more localized underneath the molecules.

The theoretical results reported in Figure 6 provide a characterization of the $(RuPc)_2$/Ag(001) system not only in terms of spatial distribution of the interface electronic states but also related to their energy position. For this reason, in Figure 7, these theoretical results are compared to the valence band spectra of the molecular layer in the low- and high-density arrangement. The photoemission spectra are complemented by the STS measurement of the 1 ML sample (high-density assembly), which allows to probe also the empty electronic states and to map the spatial distribution of electronic states along the sample surface (see also Figure S11 for a comparison of the STS to the PDOS and the i-PDOS calculated for the complete layer).

The normalized STS spectrum, obtained by averaging several spectra collected on a molecular layer (see Figure 7c for the topographic image), presents different peaks marked as F_1, F_2, and F_3 in the filled states region and E_1 and E_2 in the empty states region. At the bias voltages of the prominent peaks, differential conductance images were collected and reported in the insets of the same panel. The photoemission valence band spectrum of the 0.6 ML sample (panel b) is characterized by three peaks labeled A, B, and C. These peaks closely compare to the F_1, F_2, and F_3 features in the STS spectrum and find also a correlation with the prominent structures of the i-PDOS reported in Figure 6b for the high-density structure. However, for the 0.3 ML sample, only the B and C peaks are observed. Because these features do not disperse in angle (see Figure 4), they are expected to be contributed by the molecular states. And since theoretical results have shown negligible differences between the low- and high-density PDOS, it is reasonable to assume that differences observed between the valence bands spectra of the low- and high-density structures are due to interfacial states. Indeed, the i-PDOS plot corresponding to the low-density structure (Figure 6a) shows a strong contribution of nonresonant interfacial states in the region close to the Fermi level, which tend to smear out the resonant feature at −0.5 eV, explaining the observation of only peaks B and C in the valence band of the 0.3 ML sample.

To facilitate the comparison between i-PDOS plots and PES measurements and to explain their evolution with the molecular density, in Figure 7b simulations of the valence band spectra are reported, obtained by summing the i-PDOS to a function that mimics the photoemission contribution from the Ag(001) substrate. The signal from the substrate has been simulated by combining a Fermi step function with a polynomial function and varying the parameters in order to adjust the simulated valence band to the spectrum of the clean Ag(001) reported in Figure 4. Apart from an energy shift, our simulation recovers the three-peak structure of the 0.6 ML sample. The low-density simulation, on the other hand, shows only two structures at lower energy, in good agreement with the experimental valence band spectrum measured on the 0.3 ML sample. In fact, the electronic states around −0.5 eV in the low-density i-PDOS, corresponding to the A peak, disappear in the PES spectrum because they are incorporated by the Ag nonresonant interfacial states close to the Fermi level and by the states coming from the regions of clean Ag surface significantly present in the 0.3 ML sample. Even though the agreement between the simulated and measured spectra is only semiquantitative, the comparison in Figure 7 catches the prominent features of the interface evolution. First of all, the change in the valence band line shape between the low-density and high-density packing of the molecule is recovered. On the other hand, for the high-density structure, theoretical calculations show that around −0.5 eV (the region of the peak F_1 in STS) the i-PDOS is mainly due to molecular states, in particular the SUMO shifted below the Fermi level. This results in a three-peaks line shape in agreement with the corresponding photoemission measurements of the 0.6 ML sample. The differential conductance map of the F_1 peak shows a distribution on the surface compatible with the shape of the SUMO (see Figure 5b), confirming the assignment. Concerning the other peaks (F_3, F_2, E_1, and E_2) in the STS spectrum, theoretical calculations indicate that, except for the E_1 peak, these structures are nonresonant with molecular states. In agreement with the electronic density distribution along the interfacial plane for the nonresonant states reported in Figure 6, the differential conductance images related to these peaks are mainly gathered around the molecules. On the other hand, in the case of the resonant peak E_1, the related differential conductance image shows a clear localization underneath the

molecules, again in agreement with the results reported in Figure 6. Thus, the interface electronic states show different distributions along the plane depending on whether they are resonant with the molecular states or not.

As a last remark, we note that the relative intensity of the three peaks in the valence band (Figure 4b) changes when the molecular amount is increased from 1 to 3 ML. This behavior can be rationalized taking into account the XPS results (Figure 3) and the STM images (Figure 1). As the organic layer thickness increases, the molecules in the subsequent layers are more and more decoupled from the substrate, with the molecules in the third layer virtually decoupled from the substrate, then with an electronic structure closest to that of gas-phase molecules. The varying contribution of these molecules as the molecular amount increases can explain the evolution of the valence band line shape observed in Figure 4b. A more quantitative description of this evolution can be gained from the comparison of the molecular PDOS calculated for the gas phase and second layer molecules reported in Figure S12. It is possible to see that the molecules in the second layer present a peak of the PDOS around 1 eV justifying the higher intensity in the central peak (the B peak using the labeling in Figure 7b) in the valence band. On the other hand, the PDOS of gas phase molecules shows two structures above 1 eV and around 0.5 eV supporting the increased intensity of the peaks A and C for the 3 ML valence spectrum.

From this study emerges that a diverse charge density modulation is formed at the $(RuPc)_2$/Ag(001) interface. The molecules directly in contact with the metal present an electronic structure modified by a metal-to-molecule charge transfer which, however, appears to be independent from the molecular layer arrangement. Conversely, the different spatial distributions of the first molecular layer determine different spatial modulations and energy levels of the interface charge. Interestingly, this interface charge density presents two coexisting modulations whose periodicities are dictated by the molecular arrangement on the surface. The first one is determined by the interface electronic states resonant with the molecular orbitals. It arises from the charge accumulation underneath the molecules and the energy of the electronic states involved does not change with the molecular arrangement on the substrate. A second modulation component of the interface charge is induced by the Pauli push back phenomenon, which tends to form electronic clouds around the molecules. As a consequence, the different molecular densities on the surface induce different electrostatic interactions between the charge clouds, resulting in different energy distributions of the nonresonant electronic states. These charge modulations significantly characterize the interface electronic structure. This point can be further verified in the distribution maps of the interface electronic states in Figure 6e,f (see also Figure S9 and S10), where a careful inspection demonstrates that the interfacial density of charge even confers chiral properties to the interface as already observed in the case of the TiOPc/Ag(001) interface.[29]

CONCLUSIONS

The formation of a $(RuPc)_2$/Ag(001) interface has been thoroughly investigated using analysis tools such as STM, LEED, photoemission spectroscopy and interpreted with the help of DFT-based simulations. Our results reveal a complex landscape in which, within a few molecular layers, different assembly patterns find room, depending on the amount of deposited molecules and on their ability to exploit internal degrees of freedom to find the energetically most favored arrangement. Our approach explains why the formation of the interface is characterized at its first stages by the coalescence of just-deposited molecules and the transition between low-density and high-density ordered domains, and why it proceeds in a layer by layer mode, with the growth of second layer islands that becomes energetically favored only after the completion of the first layer in direct contact with the substrate. Of particular interest is what happens to the electronic distribution in the thin interfacial layer between molecules and substrate to drive the transition between two different ordered molecular domains on the surface. Our results disclose the atomistic structures of the two domains, having square and monoclinic structures both commensurable with the substrate, and show the set up of nondispersing states already at the first stages of the organic layer organization. However, even if individual molecules in these domains are characterized by a quite similar surface-to-molecule charge transfer pattern, the low- and high-density structures show different valence band spectra. Such differences are ascribed to the interface charge modulation along the interfacial plane. These charge modulations are governed by interfacial states energetically resonant with the molecular states, localized at the position of the molecules, as well as by a reaction of the electronic cloud of the metal surface to the molecular adsorption due to the Pauli pushback effect. These evidence demonstrate that the $(RuPc)_2$/Ag(001) is an interesting case of interaction intermediate between physisorption and chemisorption, whose spatial and energetic modulation of the interface charge layer strictly depends on the molecular assembly. Finally, the partial electronic decoupling from the surface of second-layer molecules leads into a different landscape, dominated by intermolecular interactions, where the molecules are free to arrange in a third, different square domain, incommensurable with the substrate. Overall, our results demonstrate that controlling at an atomistic or molecular level the formation of a hybrid interface requires an extremely deep understanding of all molecule−substrate, intermolecular and intramolecular interactions which, in turn, depend on the distribution in space and energy of the electrons in the whole system. This level of understanding, apparently distant from macroscopic phenomena governing the functioning of organic-electronic devices, may provide an invaluable contribution to the exploration of optoelectronic effects on a quantum scale.

ASSOCIATED CONTENT

Supporting Information

The Supporting Information is available free of charge at https://pubs.acs.org/doi/10.1021/acs.jpcc.2c08329.

Details of synthesis; Figure S1, details on the high-density structures; Figure S2, details on the low-density structures; Figure S3, Ag 3d XPS spectra; Figure S4, C 1s and Ru 3d XPS spectra raw data; Figure S5, fit of the C 1s peaks; Figure S6, ARPES measurements around the $\bar{M}$ point; Figure S7, scheme of the cells used in the DFT simulations; Figure S8, equilibrium structures calculated by DFT; Table S1, details on the density map calculations; Figure S9 and S10, complete series of density maps; Figure S11, experimental STS compared to calculate DOS; Figure S12, calculated PDOS of a gas

phase $(RuPc)_2$ molecule and placed at the second layer (PDF)

AUTHOR INFORMATION

Corresponding Authors

Giuseppe Mattioli − *Istituto di Struttura della Materia-CNR (ISM-CNR), I-00015 Monterotondo Scalo, Italy;* orcid.org/0000-0001-6331-198X; Email: giuseppe.mattioli@ism.cnr.it

Stefano Colonna − *Istituto di Struttura della Materia-CNR (ISM-CNR), I-00133 Roma, Italy;* orcid.org/0000-0001-9994-4287; Email: stefano.colonna@ism.cnr.it

Authors

Giorgio Contini − *Istituto di Struttura della Materia-CNR (ISM-CNR), I-00133 Roma, Italy*

Fabio Ronci − *Istituto di Struttura della Materia-CNR (ISM-CNR), I-00133 Roma, Italy;* orcid.org/0000-0002-7424-4046

Roberto Flammini − *Istituto di Struttura della Materia-CNR (ISM-CNR), I-00133 Roma, Italy;* orcid.org/0000-0002-2297-7221

Federico Frezza − *Istituto di Struttura della Materia-CNR (ISM-CNR), I-00133 Roma, Italy;* Present Address: Institute of Physics, Czech Academy of Sciences, 16200 Prague, Czech Republic; orcid.org/0000-0001-6511-3880

Rosanna Larciprete − *CNR-Istituto dei Sistemi Complessi, 00185 Roma, Italy;* orcid.org/0000-0002-1109-7368

Venanzio Raglione − *Istituto di Struttura della Materia-CNR (ISM-CNR), I-00015 Monterotondo Scalo, Italy;* orcid.org/0000-0003-3334-5171

Paola Alippi − *Istituto di Struttura della Materia-CNR (ISM-CNR), I-00015 Monterotondo Scalo, Italy;* orcid.org/0000-0003-4276-7501

Francesco Filippone − *Istituto di Struttura della Materia-CNR (ISM-CNR), I-00015 Monterotondo Scalo, Italy;* orcid.org/0000-0001-5862-1115

Aldo Amore Bonapasta − *Istituto di Struttura della Materia-CNR (ISM-CNR), I-00015 Monterotondo Scalo, Italy*

Gloria Zanotti − *Istituto di Struttura della Materia-CNR (ISM-CNR), I-00015 Monterotondo Scalo, Italy;* orcid.org/0000-0002-1568-3591

Bertrand Kierren − *Institut Jean Lamour, UMR 7198, CNRS-Université de Lorraine, 54011 Nancy, France*

Luc Moreau − *Institut Jean Lamour, UMR 7198, CNRS-Université de Lorraine, 54011 Nancy, France*

Thomas Pierron − *Institut Jean Lamour, UMR 7198, CNRS-Université de Lorraine, 54011 Nancy, France*

Yannick Fagot-Revurat − *Institut Jean Lamour, UMR 7198, CNRS-Université de Lorraine, 54011 Nancy, France*

Complete contact information is available at: https://pubs.acs.org/10.1021/acs.jpcc.2c08329

Notes

The authors declare no competing financial interest.

ACKNOWLEDGMENTS

We warmly thank A. M. Paoletti and G. Pennesi for invaluable discussions and their expertise in organic synthesis. The technical support by G. Emma and G. De Santis is acknowledged. S. Colonna and G. Contini acknowledge the financial support from Lorraine University (LUE-IMPACT project) for their stay in Nancy on the TUBE DAUM laboratory, during which the photoemission measurements were done. G. Contini and S.Colonna acknowledge Chiara Ceccarelli's participation in the photoemission measurements carried out at the TUBE DAUM laboratory. G. Mattioli and G. Zanotti acknowledge financial support from the Italian Ministry of the Instruction, University, and Research (MIUR) within the PRIN-2017 research program (Project 2017YXX8AZ "BOOSTER").

REFERENCES

(1) Ma, H.; Yip, H.-L.; Huang, F.; Jen, A. K.-Y. Interface Engineering for Organic Electronics. *Adv. Funct. Mater.* **2010**, *20*, 1371−1388.

(2) Kröger, I.; Stadtmüller, B.; Stadler, C.; Ziroff, J.; Kochler, M.; Stahl, A.; Pollinger, F.; Lee, T.-L.; Zegenhagen, J.; Reinert, F.; et al. Submonolayer growth of copper-phthalocyanine on Ag(111). *New J. Phys.* **2010**, *12*, 083038.

(3) Stadtmüller, B.; Kröger, I.; Reinert, F.; Kumpf, C. Submonolayer growth of CuPc on noble metal surfaces. *Phys. Rev. B* **2011**, *83*, 085416.

(4) Kröger, I.; Stadtmüller, B.; Kleimann, C.; Rajput, P.; Kumpf, C. Normal-incidence x-ray standing-wave study of copper phthalocyanine submonolayers on Cu(111) and Au(111). *Phys. Rev. B* **2011**, *83*, 195414.

(5) Bobaru, S.; Salomon, E.; Layet, J.-M.; Angot, T. Structural Properties of Iron Phtalocyanines on Ag(111): From the Submonolayer to Monolayer Range. *J. Phys. Chem. C* **2011**, *115*, 5875−5879.

(6) Stahl, U.; Gador, D.; Soukopp, A.; Fink, R.; Umbach, E. Coverage-dependent superstructures in chemisorbed NTCDA monolayers: a combined LEED and STM study. *Surf. Sci.* **1998**, *414*, 423−434.

(7) Kilian, L.; Umbach, E.; Sokolowski, M. A refined structural analysis of the PTCDA monolayer on the reconstructed Au(111) surface: Rigid or distorted carpet? *Surf. Sci.* **2006**, *600*, 2633−2643.

(8) Duhm, S.; Bürker, C.; Niederhausen, J.; Salzmann, I.; Hosokai, T.; Duvernay, J.; Kera, S.; Schreiber, F.; Koch, N.; Ueno, N.; et al. Pentacene on Ag(111): Correlation of Bonding Distance with Intermolecular Interaction and Order. *ACS Appl. Mater. Interfaces* **2013**, *5*, 9377−9381.

(9) Kilian, L.; Stahl, U.; Kossev, I.; Sokolowski, M.; Fink, R.; Umbach, E. The commensurate-to-incommensurate phase transition of an organic monolayer: A high resolution LEED analysis of the superstructures of NTCDA on Ag(111). *Surf. Sci.* **2008**, *602*, 2427−2434.

(10) Stadler, C.; Hansen, S.; Kröger, I.; Kumpf, C.; Umbach, E. Tuning intermolecular interaction in long-range-ordered submonolayer organic films. *Nat. Phys.* **2009**, *5*, 153−158.

(11) Fernandez, L.; Thussing, S.; Manz, A.; Witte, G.; Brion-Rios, A. X.; Cabrera-Sanfelix, P.; Sanchez-Portal, D.; Jakob, P. Structural and Vibrational Properties of the TiOPc Monolayer on Ag(111). *J. Phys. Chem. C* **2017**, *121*, 1608−1617.

(12) Ishii, H.; Sugiyama, K.; Ito, E.; Seki, K. Energy Level Alignment and Interfacial Electronic Structures at Organic/Metal and Organic/Organic interfaces. *Adv. Mater.* **1999**, *11*, 605−625.

(13) Zojer, E.; Taucher, T. C.; Hofmann, O. T. The Impact of Dipolar Layers on the Electronic Properties of Organic/Inorganic Hybrid Interfaces. *ACS Appl. Mater. Interfaces* **2019**, *6*, 1900581.

(14) Bagus, P. S.; Staemmler, V.; Wöll, C. Exchangelike Effects for Closed-Shell Adsorbates: Interface Dipole and Work Function. *Phys. Rev. Lett.* **2002**, *89*, 096104.

(15) Wende, H.; et al. Substrate-induced magnetic ordering and switching of iron porphyrin molecules. *Nat. Mater.* **2007**, *6*, 516−520.

(16) Zhu, X. Y. Electronic structure and electron dynamics at molecule−metal interfaces: implications for molecule-based electronics. *Surf. Sci. Rep.* **2004**, *56*, 1−83.

(17) Hofmann, O. T.; Rinke, P.; Scheffler, M.; Heimel, G. Charge Transfer and Orbital Level Alignment at Inorganic/Organic Interfaces: The Role of Dielectric Interlayers. *ACS Nano* **2015**, *9*, 5391−5404.
(18) Mattioli, G.; Mattiello, S.; Sassi, M.; Beverina, L. Ab Initio Simulations of Interfaces between SAM-Modified Gold Electrodes and n-Type or p-Type Organic Semiconductors Based on the Benzothieno-Benzothiophene (BTBT) Architecture. *J. Phys. Chem. C* **2020**, *124*, 3601−3609.
(19) Hooks, D. E.; Fritz, T.; Ward, M. D. Epitaxy and Molecular Organization on Solid Substrates. *Adv. Mater.* **2001**, *13*, 227−241.
(20) Kröger, J.; Jensen, H.; Berndt, R.; Rurali, R.; Lorente, N. Molecular orbital shift of perylenetetracarboxylic-dianhydride on gold. *Chem. Phys. Lett.* **2007**, *438*, 249−253.
(21) Kilian, L.; Hauschild, A.; Temirov, R.; Soubatch, S.; Scholl, A.; Bendounan, A.; Reinert, F.; Lee, T.-L.; Tautz, F. S.; Sokolowski, M.; et al. Role of Intermolecular Interactions on the Electronic and Geometric Structure of a Large Pi-Conjugated Molecule Adsorbed on a Metal Surface. *Phys. Rev. Lett.* **2008**, *100*, 136103.
(22) Duhm, S.; Heimel, G.; Salzmann, I.; Glowatzki, H.; Johnson, R. L.; Vollmer, A.; Rabe, J. P.; Koch, A. Orientation-dependent ionization energies and interface dipoles in ordered molecular assemblies. *Nat. Mater.* **2008**, *7*, 326−332.
(23) Chen, W.; Chen, S.; Chen, S.; Li Huang, Y.; Huang, H.; Qi, D. C.; Gao, X. Y.; Ma, J.; Wee, A. T. S. Orientation-controlled charge transfer at CuPc/F16CuPc interfaces. *J. Appl. Phys.* **2009**, *106*, 064910.
(24) Schöll, A.; Kilian, L.; Zou, Y.; Ziroff, J.; Hame, S.; Reinert, F.; Umbach, E.; Fink, R. H. Disordering of an Organic Overlayer on a Metal Surface Upon Cooling. *Science* **2010**, *329*, 303−305.
(25) Contini, G.; Gori, P.; Ronci, F.; Zema, N.; Colonna, S.; Aschi, M.; Palma, A.; Turchini, S.; Catone, D.; Cricenti, A.; et al. Chirality Transfer from a Single Chiral Molecule to 2D Superstructures in Alaninol on the Cu(100) Surface. *Langmuir* **2011**, *27*, 7410−7418.
(26) Wießner, M.; Hauschild, D.; Schöll, A.; Reinert, F.; Feyer, V.; Winkler, K.; Krömker, B. Electronic and geometric structure of the PTCDA/Ag(110) interface probed by angle-resolved photoemission. *Phys. Rev. B* **2012**, *86*, 045417.
(27) Maughan, B.; Eads, C. N.; Zahl, P.; Monti, O. L. A. Structurally induced large changes of the energy level alignment in CuPc on Cu(110)-(2× 1)O. *Phys. Rev. B* **2018**, *98*, 155106.
(28) Mattioli, G.; Larciprete, R.; Alippi, P.; Bonapasta, A. A.; Filippone, F.; Lacovig, P.; Lizzit, S.; Paoletti, A. M.; Pennesi, G.; Ronci, F.; et al. Unexpected Rotamerism at the Origin of a Chessboard Supramolecular Assembly of Ruthenium Phthalocyanine. *Chem. Eur. J.* **2017**, *23*, 16319−16327.
(29) Colonna, S.; Mattioli, G.; Alippi, P.; Amore Bonapasta, A.; Cricenti, A.; Filippone, F.; Gori, P.; Paoletti, A. M.; Pennesi, G.; Ronci, F.; et al. Supramolecular and Chiral Effects at the Titanyl Phthalocyanine/Ag(100) Hybrid Interface. *J. Phys. Chem. C* **2014**, *118*, 5255−5267.
(30) Nakashima, S.; Yamagishi, Y.; Oiso, K.; Yamada, T. K. How Contacting Electrodes Affect Single pi-Conjugated Molecular Electronic States: Local Density of States of Phthalocyanine Nanomolecules on MgO(001), Cu(111), Ag(001), Fe(001), and Mn(001). *Jpn. J. Appl. Phys.* **2013**, *52*, 110115.
(31) Sabik, A.; Trembulowicz, A.; Antczak, G. Self-organization of CoPc-F16CuPc mixture with non-equal composition on Ag(100): From sub-monolayer to monolayer coverage. *Surf. Sci.* **2021**, *705*, 121764.
(32) Al-Mahboob, A.; Sadowski, J. T. Interface energetics in zinc phthalocyanine growth on Ag(100). *Phys. Rev. B* **2016**, *93*, 085413.
(33) Armbrust, N.; Schiller, F.; Güdde, J.; Höfer, U. Model potential for the description of metal/organic interface states. *Sci. Rep.* **2017**, *7*, 46561.
(34) Colonna, S.; Zanotti, G.; Paoletti, A. M.; Pennesi, G.; Alippi, P.; Filippone, F.; Amore Bonapasta, A.; Larciprete, R.; Ronci, F.; Mattioli, G. Impact of the Substrate Work Function on Self-Assembling and Electronic Structure of Adsorbed Ruthenium Phthalocyanine. *J. Phys. Chem. C* **2020**, *124*, 23295−23306.
(35) Capobianchi, A.; Paoletti, A. M.; Pennesi, G.; Rossi, G.; Caminiti, R.; Ercolani, C. Ruthenium Phthalocyanine: Structure, Magnetism, Electrical Conductivity Properties, and Role in Dioxygen Activation and Oxygen Atom Transfer to 1-Octene. *Inorg. Chem.* **1994**, *33*, 4635−4640.
(36) Giannozzi, P.; Baroni, S.; Bonini, N.; Calandra, M.; Car, R.; Cavazzoni, C.; Ceresoli, D.; Chiarotti, G. L.; Cococcioni, M.; Dabo, I.; et al. QUANTUM ESPRESSO: a modular and open-source software project for quantum simulations of materials. *J. Phys.: Condens. Matter* **2009**, *21*, 395502.
(37) Giannozzi, P.; Andreussi, O.; Brumme, T.; Bunau, O.; Buongiorno Nardelli, M.; Calandra, M.; Car, R.; Cavazzoni, C.; Ceresoli, D.; Cococcioni, M.; et al. Advanced capabilities for materials modelling with Quantum ESPRESSO. *J. Phys.: Condens. Matter* **2017**, *29*, 465901.
(38) Cooper, V. R. Van der Waals density functional: An appropriate exchange functional. *Phys. Rev. B* **2010**, *81*, No. 161104.
(39) Thonhauser, T.; Cooper, V. R.; Li, S.; Puzder, A.; Hyldgaard, P.; Langreth, D. C. Van der Waals density functional: Self-consistent potential and the nature of the van der Waals bond. *Phys. Rev. B* **2007**, *76*, 125112.
(40) Thonhauser, T.; Zuluaga, S.; Arter, C. A.; Berland, K.; Schröder, E.; Hyldgaard, P. Spin Signature of Nonlocal Correlation Binding in Metal-Organic Frameworks. *Phys. Rev. Lett.* **2015**, *115*, 136402.
(41) Mattioli, G.; Dkhil, S. B.; Saba, M. I.; Malloci, G.; Melis, C.; Alippi, P.; Filippone, F.; Giannozzi, P.; Thakur, A. K.; Gaceur, M.; et al. Interfacial Engineering of P3HT/ZnO Hybrid Solar Cells Using Phthalocyanines: A Joint Theoretical and Experimental Investigation. *Adv. Energy Mater.* **2014**, *4*, 1301694.
(42) Vanderbilt, D. Soft Self-Consistent Pseudopotentials in a Generalized Eigenvalue Formalism. *Phys. Rev. B* **1990**, *41*, 7892−7895.
(43) Heyd, J.; Scuseria, G. E.; Ernzerhof, M. Hybrid functionals based on a screened Coulomb potential. *J. Chem. Phys.* **2003**, *118*, 8207−8215.
(44) Heyd, J.; Scuseria, G. E.; Ernzerhof, M. Erratum: "Hybrid functionals based on a screened Coulomb potential" [J. Chem. Phys. 118, 8207 (2003)]. *J. Chem. Phys.* **2006**, *124*, 219906.
(45) Janesko, B. G.; Henderson, T. M.; Scuseria, G. E. Screened hybrid density functionals for solid-state chemistry and physics. *Phys. Chem. Chem. Phys.* **2009**, *11*, 443−454.
(46) Kronik, L.; Morikawa, Y. *The Molecule-Metal Interface*; John Wiley & Sons, Ltd.: 2013; Chapter 3, pp 51−89.
(47) Hollerer, M.; Lüftner, D.; Hurdax, P.; Ules, T.; Soubatch, S.; Tautz, F. S.; Koller, G.; Puschnig, P.; Sterrer, M.; Ramsey, M. G. Charge Transfer and Orbital Level Alignment at Inorganic/Organic Interfaces: The Role of Dielectric Interlayers. *ACS Nano* **2017**, *11*, 6252−6260.
(48) Zhao, Q.; Kulik, H. J. Stable Surfaces That Bind Too Tightly: Can Range-Separated Hybrids or DFT+U Improve Paradoxical Descriptions of Surface Chemistry? *J. Phys. Chem. Lett.* **2019**, *10*, 5090−5098.
(49) Cohen, A. J.; Mori-Sànchez, P.; Yang, W. Insights into Current Limitations of Density Functional Theory. *Science* **2008**, *321*, 792−794.
(50) Mori-Sànchez, P.; Cohen, A. J The derivative discontinuity of the exchange−correlation functional. *Phys. Chem. Chem. Phys.* **2014**, *16*, 14378−14387.
(51) Hamann, D. R. Optimized norm-conserving Vanderbilt pseudopotentials. *Phys. Rev. B* **2013**, *88*, 085117.
(52) Hamann, D. R. Erratum: "Optimized norm-conserving Vanderbilt pseudopotentials" [Phys. Rev. B 88, 085117 (2013)]. *Phys. Rev. B* **2017**, *95*, No. 239906.
(53) Otani, M.; Sugino, O. First-principles calculations of charged surfaces and interfaces: A plane-wave nonrepeated slab approach. *Phys. Rev. B* **2006**, *73*, 115407.

(54) Bonnet, N.; Morishita, T.; Sugino, O.; Otani, M. First-Principles Molecular Dynamics at a Constant Electrode Potential. *Phys. Rev. B* **2012**, *109*, 115407.
(55) Haruyama, J.; Ikeshoji, T.; Otani, M. Electrode potential from density functional theory calculations combined with implicit solvation theory. *Phys. Rev. Materials* **2018**, *2*, 095801.
(56) Hermann, K.; Van Hove, M. *LEEDpat*, Version 4.2; http://www.fhi-berlin.mpg.de/KHsoftware/LEEDpat/index.html, 2014.
(57) Papageorgiou, N.; Ferro, Y.; Salomon, E.; Allouche, A.; Layet, J. M.; Giovanelli, L.; Le Lay, G. Geometry and electronic structure of lead phthalocyanine: Quantum calculations via density-functional theory and photoemission measurements. *Phys. Rev. B* **2003**, *68*, 235105.
(58) Cossaro, A.; Cvetko, D.; Bavdek, G.; Floreano, L.; Gotter, R.; Morgante, A.; Evangelista, F.; Ruocco, A. Copper-Phthalocyanine Induced Reconstruction of Au(110). *J. Phys. Chem. B* **2004**, *108*, 14671−14676.
(59) Evangelista, F.; Carravetta, V.; Stefani, G.; Jansik, B.; Alagia, M.; Stranges, S.; Ruocco, A. Electronic structure of copper phthalocyanine: An experimental and theoretical study of occupied and unoccupied levels. *J. Chem. Phys.* **2007**, *126*, 124709.
(60) Morgan, D. J. Resolving ruthenium: XPS studies of common ruthenium materials. *Surf. Interface Aanal.* **2015**, *47*, 1072−1079.
(61) Alippi, P.; Lanzilotto, V.; Paoletti, A. M.; Mattioli, G.; Zanotti, G.; Pennesi, G.; Filippone, F.; Cossaro, A.; Verdini, A.; Morgante, A.; et al. A Ru-Ru pair housed in ruthenium phthalocyanine: the role of a "cage" architecture in the molecule coupling with the Ag(111) surface. *Phys. Chem. Chem. Phys.* **2017**, *19*, 1449−1457.
(62) Weston, M.; Britton, A. J.; O'Shea, J. N. Charge transfer dynamics of model charge transfer centers of a multicenter water splitting dye complex on rutile TiO_2(110). *J. Chem. Phys.* **2011**, *134*, 054705.
(63) Henkelman, G.; Arnaldsson, A.; Jónsson, H. A fast and robust algorithm for Bader decomposition of charge density. *Comput. Mater. Sci.* **2006**, *36*, 354−360.
(64) Sanville, E.; Kenny, S. D.; Smith, R.; Henkelman, G. mproved Grid-Based Algorithm forBader Charge Allocation. *J. Comput. Chem.* **2007**, *28*, 899−908.
(65) Tang, W.; Sanville, E.; Henkelman, G. A grid-based Bader analysis algorithm without lattice bias. *J. Phys.: Condens. Matter* **2009**, *21*, 084204.